

Optimized Multi-Electrode Stimulation Increases Focality and Intensity at Target

Jacek P. Dmochowski, Abhishek Datta, Marom Bikson,
Yuzhuo Su, and Lucas C. Parra

Department of Biomedical Engineering, City College of New York–City University of
New York, New York NY, 10031

E-mail: jdmochowski@ccny.cuny.edu

Abstract. Transcranial direct current stimulation (tDCS) provides a noninvasive tool to elicit neuromodulation by delivering current through electrodes placed on the scalp. The present clinical paradigm uses two relatively large electrodes to inject current through the head resulting in electric fields that are broadly distributed over large regions of the brain. In this paper, we present a method that uses multiple small electrodes (i.e., 1.2cm diameter) and systematically optimize the applied currents to achieve effective and targeted stimulation while ensuring safety of stimulation. We found a fundamental trade-off between achievable *intensity* (at the target) and *focality*, and algorithms to optimize both measures are presented. When compared with large pad-electrodes (approximated here by a set of small electrodes covering 25 cm²) the proposed approach achieves electric fields which exhibit simultaneously greater focality (80% improvement) and higher target intensity (98% improvement) at cortical targets using the same total current applied. These improvements illustrate the previously unrecognized and non-trivial dependency of the optimal electrode configuration on the desired electric field orientation and the maximum total current (due to safety). Similarly, by exploiting idiosyncratic details of brain anatomy, the optimization approach significantly improves upon prior un-optimized approaches using small electrodes. The analysis also reveals the optimal use of conventional bipolar montages: maximally intense tangential fields are attained with the two electrodes placed a considerable distance from the target along the direction of the desired field; when radial fields are desired, the maximum-intensity configuration consists of an electrode placed directly over the target with a distant return electrode. To summarize, if a target location and stimulation orientation can be defined by the clinician, then the proposed technique is superior in terms of both focality and intensity as compared to previous solutions and is thus expected to translate into improved patient safety and increased clinical efficacy.

1. Introduction

Transcranial direct current stimulation (tDCS) is an emerging neurotechnology involving the application of small direct currents to the surface of the scalp to elicit modulation of neural activity [1]. It is currently being investigated as a therapeutic tool for a wide array of neurological conditions, including major depression [2], craving cessation [3], pain management [4]-[5], epilepsy [6], Parkinson's disease [7], and motor and speech rehabilitation after stroke [8, 9]. Moreover, tDCS has been shown to improve cognitive function, specifically memory, in healthy subjects [10, 11].

In comparison to other brain stimulation modalities such as deep brain stimulation, electro-convulsive therapy (ECT), or transcranial magnetic stimulation (TMS), the electric fields produced by tDCS are small (i.e., < 1 V/m, while other modalities are in the range of 100 V/m). Note, however, that while the resulting membrane polarization of individual cells is weak, incrementally polarizing a large population of interconnected neurons significantly alters network dynamics [12]. Moreover, the practical advantages of tDCS are great: a basic tDCS “kit” consists of a pair of electrodes, a battery, and a simple circuit capable of injecting a controlled current intensity at the anode while drawing an equivalent return current at the cathode. The procedure is inexpensive, well-tolerated, and flexible, with effects lasting well beyond the duration of the stimulation [1].

Two factors hindering the rational clinical deployment of tDCS are the limited stimulation intensities and difficulty in precisely focusing the stimulating electric fields. A significant fraction of the injected current is shunted through the scalp, thus bypassing the brain altogether and limiting the intensity of the electric field in the target region. Additionally, a lack of focal stimulation results from the diffusion of the current through the highly conductive cerebro-spinal fluid (CSF). High-resolution computational models show that CSF conducts currents to “hot-spots” that depend on the specific anatomy of the skull and idiosyncratic folding of the brain and which are not immediately apparent from the location of the electrodes on the scalp [13, 14].

In this paper, we employ precise forward-models of current flow, similar to that used to solve inverse problems in electroencephalography (EEG) analysis [15]. These models are leveraged to achieve desired electric field intensities at target brain regions while sparing other brain areas. We assume that such electric fields are well-correlated with the desired physiological changes (i.e., neuromodulation and cortical excitation or inhibition). Using a model of the human head based on Magnetic Resonance Imagery (MRI) with different conductivities for each tissue type, we numerically compute the relationship between the applied current and the resulting electric field throughout the volume of the brain. Furthermore, this computation is carried out for a specified set of electrode pairs (once for each electrode and a common reference) resulting in a linear system relating the distribution of the scalp currents to the electric field. The fields generated by each electrode pair superpose linearly. This puts the problem of achieving a desired intensity at the target while maintaining focality on solid mathematical

footing, where linear algebraic operations and efficient optimization techniques may be harnessed to derive optimal stimulation parameters. The linear superposition of the induced electric field in the brain has been leveraged previously for optimizing multi-coil transcranial magnetic stimulation (TMS) [16]. Our procedure is analogous to the problem of beamforming in array processing [17], [18] with the exception that here we must consider limits on the maximum injected current due to safety.

While the focus of this paper is on tDCS, the generalization of our optimization procedure to arbitrary input current waveforms is straightforward. For instance, sinusoidal alternating current (tACS) [19], on/off, pulsed [20] or random [21] noise stimulation have been considered. The generalization to such modalities is described in the discussion.

A critical factor that will be considered here is the maximum total current delivered to the subject. In this paper, we have chosen a sample value of 2 mA which represents a sensible and often employed safety criterion. Note, however, that tDCS safety regulations are the subject of current study [22], [23], [24]. In any case, we will show that this safety constraint (whatever value is assigned to the maximum delivered current) limits the effective degrees of freedom and thus the achieved intensity and focality. Consequently, we also report unconstrained results to determine the upper-bound on transcranial focality. Additionally, these results may be relevant for high-intensity protocols which are routinely used clinically, namely transcutaneous electrical stimulation [25] and ECT [26].

The literature on optimizing electrical stimulation is scarce; more surprising is the lack of acknowledgment of the focality problem belonging to the fundamental class of beamforming techniques. The nature of the current flow induced by tDCS has been studied in [27]–[29]. In [30], the authors search the electrode position space to locate a bipolar configuration which yields the largest current flow at the target under a total current constraint. The effect of white matter anisotropy on focality is treated in [31]. The idea of utilizing multiple electrodes for optimizing tDCS dosage has been proposed in abstract form [32].

We employ the international 10/10 electrode placement system with 64 electrodes and optimize the current applied at each electrode such that the resulting electric field is as close as possible, in a least squares sense, to a desired field. Other electrode configurations with 128 or 256 electrodes could have been used. The large number of electrode locations considered here does not mean that all electrodes will be energized. Rather, the many locations should be viewed as candidates to place a smaller number of physical electrodes. Indeed, the framework presented here will provide guidelines for selecting electrode locations even when a traditional 2-electrode configuration is used.

2. Problem Formulation

Consider a heterogeneous volume as in Figure 1 with a scalar conductivity field σ (we ignore anisotropy and assume isotropic conductivities as listed in Table 1). Because the



Figure 1. Head model segmented into various tissue categories based on T1-weighted MRI image. 64 electrodes are placed according to the international 10/10 system. Red indicates the gel between electrode (magenta) and scalp (purple). Brain shown in blue. Other tissue types given in Table 1 are omitted here for clarity.

tissue has no net current sources or sinks, the current density \mathbf{J} , inside the tissue has zero divergence: $\nabla \cdot \mathbf{J} = 0$ ($\nabla = [\frac{\partial}{\partial x}, \frac{\partial}{\partial y}, \frac{\partial}{\partial z}]$ is the gradient operator.) Thus, when applying currents through electrodes to the boundary of this volume, the resulting potential distribution V in the volume can be found as the solution to Laplace’s equation [33]:

$$\nabla \cdot \mathbf{J} = \nabla \cdot (\sigma \mathbf{E}) = -\nabla \cdot (\sigma \nabla V) = 0. \quad (1)$$

The solution is unique given that the electric field, \mathbf{E} (or equivalently, current density, \mathbf{J}) is specified at all locations on the outer boundary, and assuming continuity of electric potential and current density at tissue boundaries where conductivity changes. In general, the solution does not have a closed-form. However, a numerical approximation may be found by discretizing the volume into a set of finite elements, each with a single conductivity value, and solving (1) using finite element method (FEM) [13, 34]. In the context of tDCS, one specifies the input current density at the anode/cathode, which are placed on the boundary of the volume, and imposes zero current flow perpendicular to the surface of the scalp at all other sites (purple in Figure 1).

Consider a setup in which M electrodes and an additional (fixed) reference electrode are available (as there are 64 total electrodes in the 10/10 configuration, $M = 63$). Let \mathcal{B}_m , $m = 1, \dots, M$, denote the m th set of boundary conditions: \mathcal{B}_m consists of unit current density applied to electrode m (acting as anode), a negative unit current density at the reference electrode (acting as cathode), and zero current density perpendicular to the scalp at all other boundary locations, in particular at other electrodes. The FEM solution yields, for each \mathcal{B}_m , the effective resistivity[‡] $\mathbf{a}_m \in \mathbb{R}^3$ relating the current flowing into (out of) the anode (cathode) to the electric field $\mathbf{e}_m \in \mathbb{R}^3$ throughout the

[‡] We use the term “effective resistivity” to denote the quantity relating the magnitude of applied

tissue	conductivity (S/m)
brain	0.2
skull	0.01
CSF	1.65
scalp	0.465
muscle	0.334
air	1×10^{-15}
electrode	5.9×10^7
gel	0.3

Table 1. Conductivity values σ assigned to model components. The values are valid for DC (0 Hz) [13], [27], [29].

volume§:

$$\mathbf{e}_m(\mathbf{r}_n) = s_m \mathbf{a}_m(\mathbf{r}_n), \quad (2)$$

where $\mathbf{e}_m(\mathbf{r}_n)$ denotes the electric field vector at FEM node $\mathbf{r}_n \in \mathbb{R}^3$, $n = 1, \dots, N$, induced by stimulation of electrode m , s_m is the applied current density magnitude (for simplicity, we assume that the direction of the applied current is fixed, such as normal to the electrode surface, and work with scalar magnitudes s_m), and N is the number of FEM nodes. If we now simultaneously stimulate all electrodes such that the current density magnitude at electrode m is given by s_m , then the linearity of Laplace's equation dictates that the net electric field at location \mathbf{r}_n is given by [33]:

$$\mathbf{e}(\mathbf{r}_n) = \sum_{m=1}^M \mathbf{e}_m(\mathbf{r}_n) = \sum_{m=1}^M s_m \mathbf{a}_m(\mathbf{r}_n). \quad (3)$$

It is important to point out that the choice of a current boundary condition at the electrodes is not arbitrary: the linear superposition of the induced electric fields across separately computed anode/cathode pairs follows from the fact that the current at all other electrodes is zero. If an electric potential boundary condition is imposed at the anode, linear superposition of the separate solutions only follows if all other electrodes are explicitly grounded [35], which is more cumbersome to implement in practice.

Stacking column-wise across the discrete location space and re-writing in matrix form results in:

$$\mathbf{e} = \mathbf{A}\mathbf{s}, \quad (4)$$

current to the induced electric field. This effective resistivity is of course related to the individual resistivities (or conductivities) of the comprising tissue.

§ Given the nature of the paper, we abandon classical physics notation in favor of linear algebraic conventions, with vectors denoted by lower-case bold font and matrices with upper-case bold.

where

$$\mathbf{e} = \begin{bmatrix} \mathbf{e}(\mathbf{r}_1) \\ \mathbf{e}(\mathbf{r}_2) \\ \vdots \\ \mathbf{e}(\mathbf{r}_N) \end{bmatrix}, \quad \mathbf{A} = \begin{bmatrix} \mathbf{a}_1(\mathbf{r}_1) & \mathbf{a}_2(\mathbf{r}_1) & \cdots & \mathbf{a}_M(\mathbf{r}_1) \\ \mathbf{a}_1(\mathbf{r}_2) & \mathbf{a}_2(\mathbf{r}_2) & \cdots & \mathbf{a}_M(\mathbf{r}_2) \\ \vdots & \vdots & \ddots & \vdots \\ \mathbf{a}_1(\mathbf{r}_N) & \mathbf{a}_2(\mathbf{r}_N) & \cdots & \mathbf{a}_M(\mathbf{r}_N) \end{bmatrix}, \quad \mathbf{s} = \begin{bmatrix} s_1 \\ s_2 \\ \vdots \\ s_M \end{bmatrix}.$$

The net electric field is a linear combination of the individual electric fields yielded by each bipolar configuration as computed by the FEM solver. It is clear that the nature of the field is intimately related to the individual current densities s_m . This fact allows us to tune these current densities such that the resulting field is optimal with respect to a specified measure. With M stimulating electrodes (“anodes”), we have M degrees of freedom at our disposal: the current density at the reference electrode (“cathode”) is given by $-\sum_m s_m$. Since the value of s_m need not be positive, current may flow out of any of the M electrodes (thus acting as a cathode). The problem of choosing the coefficients s_m to shape the induced field is analogous to the “beamforming” problem in array signal processing. For example, an array of microphones may be steered to form an acoustic beam to a desired direction of arrival [17], [18] – the diversity of multiple microphones is leveraged to form a directional response. In our framework, the columns of \mathbf{A} represent linearly independent “paths” which may be intelligently combined to yield a maximally focal (or intense) net electric field at the target (Figure 2). In the following section, we propose several optimization schemes suitable for optimizing non-invasive electrical stimulation modalities.

3. Optimization Schemes

3.1. Least Squares

The well-known least-squares approach is concerned with selecting a parameter to minimize a second-order error term. Denote the desired electric field by $\mathbf{e}_d(\mathbf{r}_n) \in \mathbb{R}^3$, which takes relatively large values at positions near the target. Brain areas which we want to leave unaffected by the stimulation are assigned a zero value. A logical choice for the desired field is thus given by:

$$\mathbf{e}_d(\mathbf{r}_n) = \begin{cases} \mathbf{e}_o & n \in \mathcal{T} \\ 0 & n \in \mathcal{T}^c \end{cases}, \quad \mathbf{e}_d = \begin{bmatrix} \mathbf{e}_d(\mathbf{r}_1) \\ \mathbf{e}_d(\mathbf{r}_2) \\ \vdots \\ \mathbf{e}_d(\mathbf{r}_N) \end{bmatrix}, \quad (5)$$

where \mathbf{e}_o defines the desired orientation and intensity of the target region, \mathcal{T} is a set of nodes defining the target region, and \mathcal{T}^c is the set complement of \mathcal{T} . A sensible choice for the direction specified by \mathbf{e}_o is radial or tangential to the skull surface, particularly in the case of cortical stimulation.

Minimizing the squared error between the desired field and that which is achievable

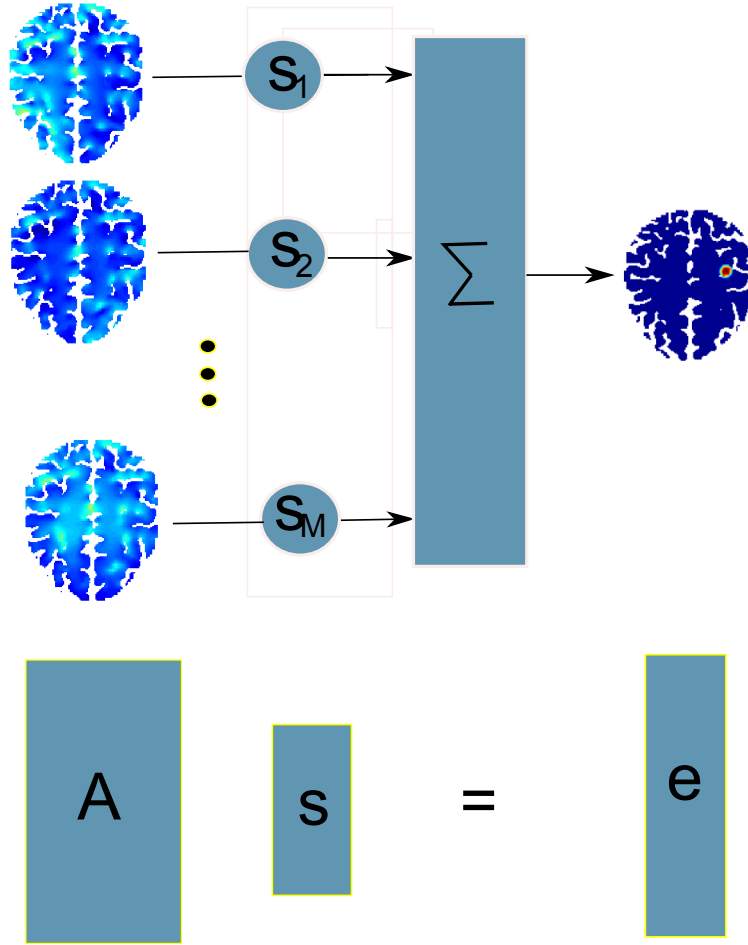


Figure 2. Combining component fields linearly to achieve desired field distribution and strength.

by the linear superposition of (4) leads to the well-known least squares solution:

$$\begin{aligned} \mathbf{s}_{\text{ls}} &= \arg \min_{\mathbf{s}} \|\mathbf{e}_d - \mathbf{A}\mathbf{s}\|^2 \\ &= (\mathbf{A}^T \mathbf{A})^{-1} \mathbf{A}^T \mathbf{e}_d. \end{aligned} \quad (6)$$

Geometrically, \mathbf{s}_{ls} is the vector in the span of the columns of \mathbf{A} with minimum Euclidean distance to \mathbf{e}_d – unfortunately, the solution of (6) is generally unsuitable, as the obtained current densities are free to take values outside of the allowable range for safety. In conventional bipolar tDCS, the amount of current through any one electrode is constrained to I_{max} , with a typical value of I_{max} being 2 mA. Denoting the (fixed) electrode area by A , we analogously define $s_{\text{max}} = I_{\text{max}}/A$. It is not straightforward to extend this safety constraint to multiple electrode stimulation. The safest approach is to limit the sum of all positive currents (i.e., the total current delivered) to I_{max} . (An alternative would be to limit the current at each electrode individually; this will be discussed in more detail in section 3.2). Since the sum of positive currents equals the sum of negative currents, this is equivalent to limiting the sum of absolute values of all currents to $2I_{\text{max}}$.

Moreover, note that the number of total nodes N is quite large due to the need to finely sample \mathcal{V} in order to compute accurate FEM solutions – one can easily expect N to be in the order of 10^5 . On the other hand, given that the brain regions which we want to stimulate have a small spatial extent, the number of nodes in \mathcal{T} is expected to be low (i.e., in the order of 10). The objective function $\|\mathbf{e}_d - \mathbf{A}\mathbf{s}\|^2$ is a summation of squared errors across all nodes:

$$Q \triangleq \|\mathbf{e}_d - \mathbf{A}\mathbf{s}\|^2 = \sum_{n \in \mathcal{T}} \left\| \mathbf{e}_o - \sum_{m=1}^M \mathbf{a}_m(\mathbf{r}_n) s_m \right\|^2 + \sum_{n \in \mathcal{T}^c} \left\| \sum_{m=1}^M \mathbf{a}_m(\mathbf{r}_n) s_m \right\|^2. \quad (7)$$

It is thus apparent that minimizing the sum of squared errors leads to an inherent trade-off between achieving the required intensity in \mathcal{T} while keeping the field minimal in \mathcal{T}^c – focality. In order to control this trade-off, consider writing the weighted sum of squares as:

$$Q_w \triangleq w \sum_{n \in \mathcal{T}} \left\| \mathbf{e}_o - \sum_{m=1}^M \mathbf{a}_m(\mathbf{r}_n) s_m \right\|^2 + w^c \sum_{n \in \mathcal{T}^c} \left\| \sum_{m=1}^M \mathbf{a}_m(\mathbf{r}_n) s_m \right\|^2, \quad (8)$$

where w and w^c are linear weights such that $\frac{w|\mathcal{T}|}{w^c|\mathcal{T}^c|} = k$, where $|\cdot|$ is the cardinality of a set. The constant k is a scalar controlling the trade-off between intensity and focality. When $k = 1$, the weights w and w^c act to counterbalance the asymmetry in the number of target and non-target nodes. A large value of k forces the optimization to emphasize attaining the desired intensity in the target region. A low value of k emphasizes nulling the non-target regions.

Define the diagonal matrix $\mathbf{W} \in \mathbb{R}^{3N \times 3N}$, whose n th nonzero element is given by:

$$[\mathbf{W}]_n = \begin{cases} w & [n/3] \in \mathcal{T} \\ w^c & [n/3] \in \mathcal{T}^c \end{cases}, \quad (9)$$

where $[\cdot]$ rounds the argument to the nearest integer. In conjunction with the safety condition, the resulting constrained optimization problem is written as:

$$\mathbf{s}_{\text{wls-con}} = \arg \min_{\mathbf{s}} \|\mathbf{W}^{1/2} (\mathbf{e}_d - \mathbf{A}\mathbf{s})\|^2 \quad \text{subject to} \quad \sum_m |s_m| + \left| \sum_m s_m \right| \leq 2s_{\text{max}}. \quad (10)$$

Note that $\sum_m |s_m| = \|\mathbf{s}\|_1$ is by definition the ℓ_1 norm of the current density vector (the term $|\sum_m s_m|$ accounts for the current through the reference electrode). There is no closed-form solution to ℓ_1 norm constrained least squares, and iterative procedures must be employed to solve (10). An efficient algorithm for solving this problem is known as the Least Absolute Shrinkage and Selection Operator (LASSO) algorithm [36]. Least-squares optimization with an ℓ_1 norm constraint is popular due to the fact that the resulting solutions often exhibit sparseness. Thus, by limiting the maximum total current we are not only satisfying a sensible safety constraint but also encouraging solutions in which a majority of the current is being guided through just a few electrodes. This has the advantage of potentially requiring simpler stimulation hardware with fewer independent current-control channels.

3.2. Weighted Least-Squares with Individual ℓ_1 Constraint

The safety constraint limiting total current is guided by the notion that the effect of the injected current is globally additive. However, this may not be an accurate representation of the safety limitations of electrical stimulation as some electrode configurations may act only locally; for example, bipolar electrodes on one side of the head will not affect brain tissue on the other side of the head. In this case, a more local safety constraint guided by skin reactions and sensation levels directly under each electrode may be more appropriate. In those cases, it may be suitable to relax the safety constraint on $\|\mathbf{s}\|_1$ and rather limit the absolute value of the current at each individual electrode. Such a procedure may be especially valid if the set of electrodes are a considerable distance apart. The corresponding optimization problem is written as:

$$\begin{aligned} \mathbf{s}_{\text{wls-ind}} = \arg \min_{\mathbf{s}} \left\| \mathbf{W}^{1/2} (\mathbf{e}_d - \mathbf{A}\mathbf{s}) \right\|^2 \text{ subject to } |s_m| \leq s_{\text{max}}, \forall m, \\ \text{and } \left| \sum s_m \right| \leq s_{\text{max}}. \end{aligned} \quad (11)$$

The solution to (11) may be found numerically via an iterative algorithm. As the numerical evaluations will show, the resulting electric fields are more intense than those produced by (10), but at the expense of larger current flowing through the brain. In addition, the resulting scalp current distributions are more broadly distributed than with the ℓ_1 norm constraint.

The weighted least-squares (WLS) approach requires the clinician to specify a desired field in addition to assigning a weight to each node's error term. It is not straightforward to relate the value of k to the resulting intensity obtained by the optimization. In the absence of a closed-form solution, the value of k must be iteratively adjusted until the desired intensity is produced by the optimization. To alleviate this computational burden, we propose an alternative to least-squares optimization below.

3.3. Linearly Constrained Minimum Variance

In the beamforming literature, a common scheme is to enforce a hard linear constraint (e.g., enforce a desired gain for a given direction) while utilizing the remaining degrees of freedom to minimize the total power. Analogously, here we want to achieve a specified electric field at a single node while minimizing the electric field elsewhere. Such a procedure does not require any weighting, and the hard constraint ensures that we attain the desired field at the target. From all current distributions \mathbf{s} that satisfy the hard constraint, the linearly constrained minimum variance (LCMV) procedure selects the one with the lowest overall electric field power $\|\mathbf{A}\mathbf{s}\|^2$ across the volume:

$$\mathbf{s}_{\text{lcmv}} = \arg \min_{\mathbf{s}} \|\mathbf{A}\mathbf{s}\|^2 \text{ subject to } \mathbf{C}\mathbf{s} = \mathbf{e}_o, \quad (12)$$

where

$$\mathbf{C} = \begin{bmatrix} \mathbf{a}_1(\mathbf{r}_{n_o}) & \mathbf{a}_2(\mathbf{r}_{n_o}) & \cdots & \mathbf{a}_M(\mathbf{r}_{n_o}) \end{bmatrix}, \quad (13)$$

and n_o is the index of the target node. The solution to (13) follows from the method of Lagrange multipliers as [37]:

$$\mathbf{s}_{\text{lcmv}} = (\mathbf{A}^T \mathbf{A})^{-1} \mathbf{C}^T \left[\mathbf{C} (\mathbf{A}^T \mathbf{A})^{-1} \mathbf{C}^T \right]^{-1} \mathbf{e}_o. \quad (14)$$

The LCMV technique is attractive as the clinician need only specify the target node and the desired field at that node. However, note that there are no guarantees that the resulting electric field exhibits a maximum at the target; on the contrary, a known drawback of LCMV is that undesired “side-lobes” are formed at non-target areas. This is the price to be paid for ensuring the exact desired field strength and orientation at the target. Moreover, if the desired intensity at the target node is chosen to be too large, the required currents may violate the safety criteria; in this case, a lower value for the target intensity must be chosen.

To ensure safety of stimulation, the ℓ_1 constrained LCMV problem follows as:

$$\mathbf{s}_{\text{lcmv-con}} = \arg \min_{\mathbf{s}} \|\mathbf{A}\mathbf{s}\|^2 \text{ subject to } \mathbf{C}\mathbf{s} = \mathbf{e}_o \text{ and } \sum_m |s_m| + \left| \sum_m s_m \right| \leq 2s_{\text{max}}, \quad (15)$$

for which an iterative solution may be found using conventional numerical methods (see section 5).

Similarly, the individually ℓ_1 constrained LCMV problem is written as:

$$\begin{aligned} \mathbf{s}_{\text{lcmv-ind}} = \arg \min_{\mathbf{s}} \|\mathbf{A}\mathbf{s}\|^2 \text{ subject to } \mathbf{C}\mathbf{s} = \mathbf{e}_o \text{ and } |s_m| \leq s_{\text{max}}, \forall m, \\ \text{and } \left| \sum s_m \right| \leq s_{\text{max}}, \end{aligned} \quad (16)$$

3.4. Optimizing for Intensity

The optimization of focality corresponds to maximizing tDCS safety, as undesired brain regions are spared by the stimulation. In some cases, it may be desirable to sacrifice focality and rather maximize the electric field at the target location. The framework of (4) easily allows one to formulate the problem of optimizing intensity: recall from (13) that \mathbf{C} consists of the rows of \mathbf{A} corresponding to the target node, while \mathbf{e}_o denotes the desired field orientation at the target. Thus, the maximization of the intensity in the desired direction at the target takes the form of a linear programming problem [38]:

$$\mathbf{s}_{\text{max}} = \arg \max_{\mathbf{s}} \mathbf{e}_o^T \mathbf{C}\mathbf{s} \text{ subject to } \sum |s_m| + \left| \sum s_m \right| \leq 2s_{\text{max}}, \quad (17)$$

where it should be noted that $\mathbf{e}_o^T \mathbf{C}\mathbf{s}$ is the projection of the electric field at the target node on a vector pointing in the direction of the desired field.

4. Performance Metrics

In order to assess the focality of a given field, we define the following metric which quantifies the proportion of the electric field magnitude contained within a sphere of increasing radius around the target:

$$\mathcal{F}(r) = \frac{\sum_{n \in \mathcal{T}(r)} \|\mathbf{e}(\mathbf{r}_n)\|}{\sum_n \|\mathbf{e}(\mathbf{r}_n)\|}, \quad (18)$$

where $\mathcal{T}(r)$ is a set consisting of all nodes within radius r of the target node. We define the “half-max-radius” (analogous to the full-width-half-max) as the radius which contains half of the total electric field:

$$r_{0.5} \triangleq r | \mathcal{F}(r) = 0.5. \quad (19)$$

An example for $\mathcal{F}(r)$ and $r_{0.5}$ is given in Figure 6a. A plot of $r_{0.5}$ for varying desired target intensities characterizes an algorithm’s ability to yield focal electric fields across a range of intensities (e.g., Figure 7c). In the forthcoming results, we plot the half-max radius against the target intensity in the desired direction (i.e., the projection of the electric field at the target onto a unit vector pointing in the specified orientation). For the ℓ_1 norm constrained LCMV method (15), this curve terminates at the maximum intensity that can be achieved at the target without violating the safety constraint.

Note that $\mathcal{F}(r)$ is entirely independent of field direction: thus, we also report the angular misalignment between actual and desired field directions at the target node: the hard constraint of the LCMV scheme guarantees that this error will be zero. On the other hand, the weighted least squares and maximum intensity methods will lead to a disparity between the desired and actual field orientations at the target.

The results will be compared to simulated large pad-electrodes. A pad-electrode is simulated, or sampled, as a square arrangement of 5 small electrodes (approximately 5 cm side-length; see Figures 8 and 9). Note that the field generated by this simulated montage is expected to differ somewhat to that produced by actual pad-electrodes. However, this discrepancy is expected to be small.

Small electrodes allow for better control of the resulting field orientation as compared to large pads. To evaluate the relative merits of optimization over the use of small electrodes, we also compare to current ad-hoc approaches for placing electrodes to achieve desired tangential and radial current directions. When specifying tangential current flow, the optimized results are compared to a bipolar configuration in which adjacent electrodes are oriented in the desired direction. In the case of a radial desired field, the benchmark will be the “4-by-1” configuration [13], in which the anode is surrounded by 4 cathodes. For the sake of clarity, we refer to these benchmark configurations as “ad-hoc”; however, it should be noted that they do represent the conventional configuration for tDCS montages.

5. Computational Workflow

The anatomical model was derived from an MRI of the head of a 35-year old healthy male recorded with a 3T Philips Achieva scanner (Philips Medical Systems, Amsterdam, Netherlands). The acquisition matrix has size 256-by-256-by-190 with a voxel size of 1mm-by-1mm-by-1mm. The image is then automatically segmented into four tissue categories (brain, CSF, scalp, and skull) using FSL’s Brain Extraction Tool and Automated Segmentation Toolbox (FSL, Oxford, UK). The model is then fitted with electrodes placed on the scalp according to the international 10/10 system (electrode

distance is 10% of the circumference from nasion to inion and from left to right preauricular points); each electrode is modeled as a cylinder of 12mm diameter and 2mm depth. Additionally, conducting gel with a 1mm thick layer and surface area equal to that of the cylinder rests directly under the electrode. Manual correction of the automated segmentation is then performed using Simpleware's ScanIP tool (Simpleware, Exeter, UK), followed by further segmentation of the volume into the following categories: electrode, conducting gel, brain, CSF, skull, scalp, air, and muscle. The segmented head is shown in Fig. 1. The labeled volume is then translated to a finite element mesh using Simpleware's ScanFE software and isotropic conductivity values are assigned to each tissue type following Table 1.

Laplace's equation (1) is solved in Abaqus (Simulia, Providence, RI) by fixing one electrode as the reference cathode (i.e., Iz), grounding the chosen reference, and then stimulating a single electrode with an input current density of 1 A/mm²; this current density was applied uniformly to the outer surface of the electrode. This procedure is repeated for all $M = 63$ free electrodes to yield the mixing matrix \mathbf{A} . Note that due to the explicit modeling of the electrode, gel, and scalp interfaces, the application of a uniform current density at the surface results in greater current density at the edges of the conductive gel and scalp, as expected given the physical laws of current flow and the results of previous studies [39].

The optimization of currents was performed in MATLAB (Mathworks, Natick, MA) using disciplined convex programming [40]. In all cases, only the nodes corresponding to the brain were employed for the optimization. Note that all optimization schemes considered constitute a convex optimization problem. It should be pointed out that the optimization may be facilitated by considering the singular value decomposition [41] of the mixing matrix: $\mathbf{A} = \mathbf{U}\mathbf{D}\mathbf{V}^T$, where $\mathbf{U} \in \mathbb{R}^{N \times M}$ and $\mathbf{V} \in \mathbb{R}^{M \times M}$ are orthonormal and $\mathbf{D} \in \mathbb{R}^{M \times M}$ is diagonal. Note that:

$$\begin{aligned} \arg \min_{\mathbf{s}} \|\mathbf{e}_d - \mathbf{A}\mathbf{s}\|^2 &= \arg \min_{\mathbf{s}} \|\mathbf{U}^T(\mathbf{e}_d - \mathbf{A}\mathbf{s})\|^2 \\ &= \arg \min_{\mathbf{s}} \|\mathbf{U}^T\mathbf{e}_d - \mathbf{D}\mathbf{V}^T\mathbf{s}\|^2, \end{aligned} \quad (20)$$

with the dimensionality of the problem in (20) equaling M . Thus, by minimizing the projection of the field error vector on the columns of \mathbf{U} , one obtains the solution to the original optimization while greatly minimizing computational time (a factor of 10^3 in our case). Similarly, note that:

$$\|\mathbf{A}\mathbf{s}\|^2 = \|\mathbf{D}\mathbf{V}^T\mathbf{s}\|^2, \quad (21)$$

and thus the LCMV optimization schemes may equivalently minimize the inner product on the right of (21).

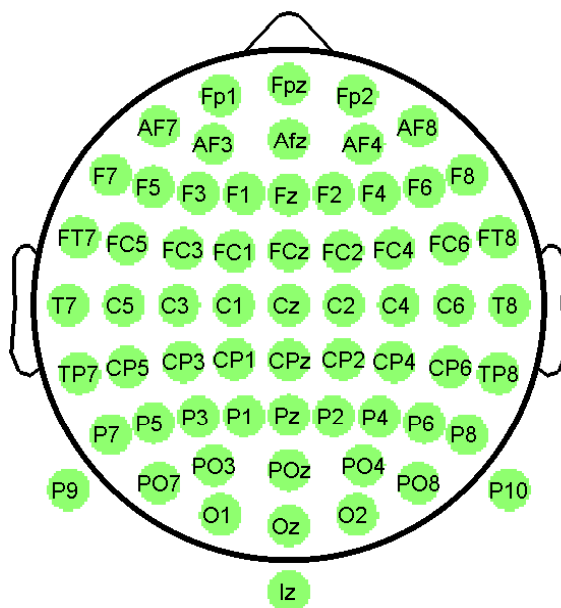


Figure 3. Two dimensional visualization of the standard 10/10 electrode arrangement.

6. Results

6.1. Optimal solution varies non-trivially with the desired orientation and criterion

To illustrate the strong dependence of the optimal currents on the desired orientation, we select a target located on a gyrus on the posterior side of the central sulcus, and then compute the optimal solutions in both radial and tangential directions, as shown in Figures 4a and b. Moreover, we optimize for both focality (LCMV- ℓ_1 with a target intensity of 0.1 V/m) and intensity, yielding four total solutions, which are illustrated in Fig. 4c-f. The current distributions are displayed using a modified version of the EEGLAB’s `topoplot` function which renders the applied scalp currents (in EEG analysis, the values typically represent recorded electric potentials) in two dimensions [42] using the conventional schematic for the 10/10 international system (Figure 3). In the forthcoming results, each electrode is represented with a circle whose color indicates the amount of current injected into that electrode (in units of mA).

The disparity between the optimal currents for the various orientations/criteria is apparent. In the radial case, the maximally focal solution takes the form of a positive two-electrode “pad” over the target, with six surrounding electrodes employed for the return currents. This configuration may be thought of as an “elongated 4-by-1” (compare with Figure 8d). On the other hand, when desiring tangential current flow,

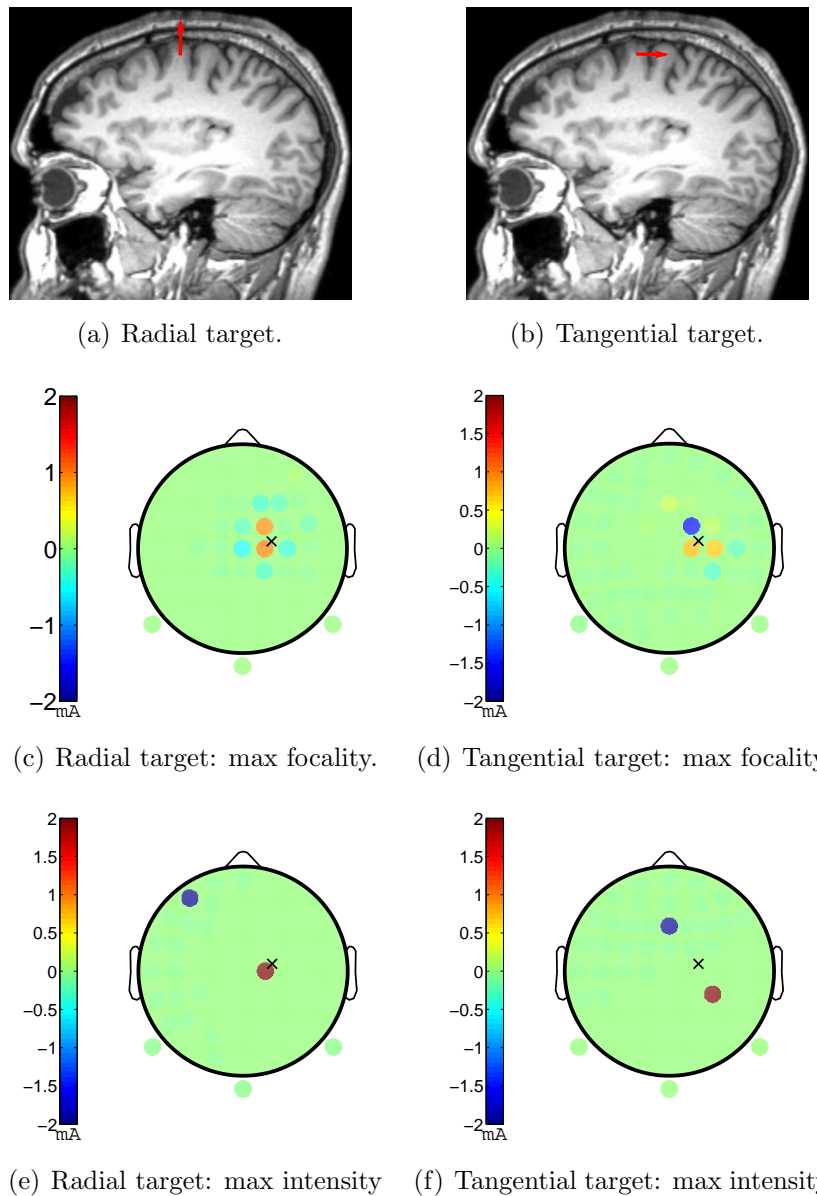


Figure 4. Optimal current distribution as a function of desired orientation and criterion.

the optimal currents are defined by a two-electrode anode, with a strong one-electrode return, in addition to weaker components adjacent to the anode and cathode. Note the close proximity of the major stimulating and return electrodes. This is in stark contrast to the maximally intense solutions (sub-figures e and f), which take the form of a semi-distant bipolar configuration – note that maximum target intensity does not arise by spacing the electrodes maximally apart, as intuition may suggest. It is also important to point out that the optimal placement of the two electrodes is dependent on the desired field orientation at the target: in the radial case, the anode is placed directly over the target. On the other hand, in the tangential case, the target lies between the anode and cathode.

Figure 5 displays the coronal, sagittal, and axial slices of the resulting electric field intensity and orientation. These slices intersect the target location^{||}. The half-max radii of the focality optimized radial and tangential schemes are 44mm and 46mm, respectively (each with a target intensity of 0.1 V/m as specified by the hard constraint). Note that the maximum electric field occurs at a region nearby, but not precisely at, the target. This is in part a drawback of LCMV, but mostly stems from physical limitations imposed by the laws of volume conduction and encapsulated by the properties of the forward-model matrix \mathbf{A} . The maximum intensities yielded for the radial and tangential targets are 0.3 V/m and 0.35 V/m; in general, we have observed that larger optimized target intensities are attainable with tangential stimulation. We summarize the results in Figure 6, which also displays $\mathcal{F}(r)$ for the radial case when optimizing for focality with the half-max radius indicated.

6.2. WLS attains greater focality than LCMV at the expense of misaligned field direction at target

We compare the ℓ_1 norm constrained LCMV and WLS schemes in terms of the intensity-focality trade-off for two targets: a gyrus anterior of the central sulcus for which we specify radial field direction (Fig. 7a), and the anterior side of the central sulcus for which we desire tangential current flow (Fig. 7b). Orientations are selected to be perpendicular to the cortical sheet as polarization of pyramidal cell somata is maximal with such orientation [43]. Figures 7c-d depict the intensity-focality curves yielded by both algorithms for a range of specified intensities: for the LCMV- ℓ_1 method (15), the intensity range varies from 0.01 to 0.17 V/m in increments of 0.01 – fields beyond 0.17 V/m can not be attained when limiting the total current to 2mA. For the safety constrained WLS solution of (10), the value of k values varies logarithmically from 10^{-4} to 10^1 in 50 increments – these values resulted in a range of target intensities comparable to the LCMV intensity range. Figures 7e-f depict the misalignment in field direction at the target for both methods.

In the case of radial stimulation, the two methods yield virtually equivalent focality across the obtained intensity range, with a slight separation in $r_{0.5}$ occurring near 0.15 V/m. When desiring tangential current flow, a more significant focality increase is attained by WLS above 0.15 V/m. Note that the LCMV feasible range is much broader (up to 0.37 V/m) in the tangential case than that of the radial target (0.17 V/m). Moreover, the WLS scheme yields intensities significantly beyond the LCMV feasible range with tangential stimulation. Note that while the WLS problem is feasible for all target intensities, the achievable intensity is of course limited by the safety constraints. From Fig. 7f, it is also interesting to point out that the error in WLS field direction

^{||} When showing the slices, we have used the radiological convention of displaying the slices from the vantage point of the clinician facing the patient. Note that the visualization of the scalp currents is thus flipped left-to-right with respect to the axial electric field slice. Moreover, since the range of field intensities varies greatly across techniques, we chose to employ separate color map limits for each method, while enforcing the same limits within each method across the three slices.

begins to rise sharply at approximately the intensity at which LCMV becomes infeasible: the optimization algorithm is limited in its degrees of freedom, and thus resorts to a greater angular mismatch in order to attain the desired target intensity.

In summary, irrespective of the algorithms used or the desired field direction, as the achievable intensities increase, the fields become more broadly distributed.

6.3. Intensity and focality can be substantially improved over conventional approaches

To quantify the benefits of optimizing the applied currents and to establish an upper bound on achievable intensity and focality, we choose a cortical target for which we specify both radial (Fig. 8a) and tangential stimulation (Fig. 9a). We then compute the half-max radii and the feasible target intensities for a range of electrode montages and optimization criteria: simulated large-pad electrodes (5 electrodes of same polarity), two “ad-hoc” small electrode arrangements (4-by-1 or bipolar), and small-electrode arrays optimized for focality with the ℓ_1 norm constraint (15) “LCMV- ℓ_1 ”, optimized for focality with the individual ℓ_1 constraint (16) “LCMV-ind”, optimized for focality without safety constraint (14) “LCMV”, and optimized for intensity irrespective of focality (17) “Max Intensity”. Figures 8b and 9b depict the focality-intensity curves for the radial and tangential directions, respectively. Additionally, we show the coronal slice of the electric fields and optimal current distributions for all six schemes in Figures 8c-h (radial) and 9c-h (tangential) – for all focality optimized schemes, the coronal slices are shown for a target intensity of 0.16 V/m (0.23 V/m) in the radial (tangential) case.

Radial fields with target underneath the electrode

Beginning with the radial case, note that with the simulated pad montage, the field intensity at the target is 0.16 V/m with a half-max radius of 80mm. Meanwhile, the ad-hoc 4-by-1 configuration attains the same target intensity with an $r_{0.5}$ of 57mm. Immediately, the benefits of optimizing for focality become apparent, as the LCMV- ℓ_1 scheme achieves field intensities of up to 0.25 V/m, while maintaining a half-max radius less than 69mm. At the intensity attained by the simulated pad and ad-hoc schemes (0.16 V/m), the LCMV- ℓ_1 method yields a 80% improvement in focality over the pads and 47% over the ad-hoc scheme. We define the improvement as the percentage decrease in the volume containing half of the electric field ($\propto r_{0.5}^3$).

As expected due to the increased degrees of freedom, the LCMV with currents constrained at each electrode exhibits an excellent focality-intensity trade-off: $r_{0.5}$ of 40mm at 0.3 V/m. Most striking is the fact that the the LCMV method with unconstrained currents achieves a half-max radius of only 30mm – note that only the magnitude, and not the distribution of the optimal unconstrained currents (14) change with an increased target intensity; thus, $r_{0.5}$ remains constant. Turning to Figure 8g, we observe that this unconstrained solution resembles a “spherical sinc” function, with rings of alternating polarity centered over the target. This finding resembles theoretical

calculations on spherical head-models (Dmochowski, unpublished) and supports the efficacy of the experimentally obtained 4-by-1 montage.

It is interesting to note that the LCMV- ℓ_1 solution (Figure 8e) is a non-trivially modified version of the ad-hoc 4-by-1, with the difference being the location and magnitude of the return electrodes. This slight difference accounts for a significant reduction in half-max radius. Herein lie the benefits of performing a patient-specific optimization of the applied currents: the nominal 4-by-1 arrangement is only an approximation to the ideal solution (the unconstrained LCMV), and the idiosyncrasies of patient anatomy are indispensable to the computation of the maximally focal configuration (i.e., which electrodes to use as the returns, and how much current to pass through them). The sensitivity of focality to deviations from the optimal current distribution is analogous to the problem of desired signal cancellation in array beamforming [44], in which slight movement of the signal source leads a large decrease in signal quality. In our case, the optimization of the electric field focality relies strongly on the cancellation of the field outside of the target node via weighted subtraction of the columns of \mathbf{A} . However, the outcome of this weighted subtraction is very sensitive to the weights and columns used.

Finally, the maximum intensity scheme yields a target intensity of 0.31 V/m, representing a 97% (98%) improvement in achieved target intensity over the simulated pad (ad-hoc 4-by-1) montage, while using the same amount of input current. From Figure 8h, it is obvious that any attempt to maximize target intensity compromises focality, and the intensity optimized configuration takes the form of a “semi-distant” bipolar, with the anode placed directly over the target. Due to the lack of symmetry in the montage, the resulting electric field lacks focality and leads to the introduction of several undesirable “hot-spots.” The optimization scheme here serves to identify the most intense bipolar configuration based on individual patient anatomy, the safety constraint, and the desired field orientation.

Tangential fields with targets between electrodes

Consider now Figure 9b, which details the focality-intensity trade-off in the case of tangential stimulation. In this case, the simulated pad and ad-hoc bipolar montages attain target intensities of 0.23 and 0.29 V/m and half-max radii 80 and 69mm, respectively. At 0.23 V/m, the ℓ_1 norm constrained solution yields an improvement of 52% in focality over the simulated pad scheme. Moreover, the improvement over the ad-hoc bipolar montage at 0.29 V/m is 12%. The reduced improvement in focality compared to the radial case may be attributed to the fact that tangential stimulation leads to larger target intensities – at these larger intensities, there are fewer degrees of freedom available to the optimization schemes, and thus only moderate gains in focality are observed.

The individually ℓ_1 constrained and unconstrained LCMV solutions yield massive improvements over conventional methods, with the half-max radius not exceeding 45mm

at 0.29 V/m. Note that the safety-unconstrained currents resemble a spherical sinc with non-arbitrary weights applied to the involved electrodes and an additional ring emerging (compared to the radial case). It is difficult to find structure in the individually ℓ_1 constrained optimal current configuration.

In terms of target intensity, the maximum intensity scheme yields a target intensity of 0.48 V/m, representing an improvement of 63% and 112%, respectively, over the simulated pad and ad-hoc bipolar montages. The maximally intense montage is bipolar with the pair of electrodes arranged in the direction of desired orientation, and the target resting between the electrodes. Here again, the optimization's role is not in determining amount of current injected, but rather the location of the bipolar montage.

7. Discussion

7.1. Robustness

It remains to be established whether the observed increases in intensity and focality are robust to errors in electrode placement or to errors in the segmentation and modeling of electrical properties of tissue. For instance, anisotropic conductivity in white-matter tracts may affect the precise flow of currents in the brain [31]. Regardless, the framework established here can straightforwardly incorporate such improved modeling efforts. It should also be straightforward to carry out a robustness analysis within the present framework, either analytically by considering small perturbations on electrode location or segmentation errors using linearized sensitivity analysis or by means of explicit numerical simulations of perturbations.

7.2. Clinical relevance of targeting

At present, many clinical trials have no well-defined target areas and the anatomical substrates of trials using pad-electrodes have to be interpreted with caution in light of the limited focality and misconceptions on the location of maximum stimulation (discussed above, but see also [13]). Until further clarity emerges on the desired target locations for specific conditions, it may be that focal stimulation is not desirable: if the target is not known, it may be better to stimulate broadly and rely on the behavioral paradigm for specificity. However, if efficacy and safety are to be systematically optimized, we believe that it is paramount to identify the precise site of action of electrical stimulation paradigms – once target locations can be defined, the present results justify the increased complexity in software and hardware required for targeting. Incidentally, our broader goal is to fully automate the modeling process, encompassing the segmentation of the MRI image, electrode placement, FEM meshing, solving of multiple electrode pairs and optimization. At the end of this automated processing, the clinician is only required to select a target location and orientation.

7.3. Clinical relevance of radial and tangential field orientation

Significant experimental work is still outstanding to establish whether orientation of stimulation matters in practice. Radial and tangential directions were defined here relative to the skull as this surface is the major determinant for placing electrodes. From a functional point of view, the target direction will likely be defined based on the cortical anatomy, which due to its extensive folding, does not necessarily correspond to the simple tangential or radial directions defined here. In our examples, however, we ensured that stimulation orientations were in fact perpendicular to the cortical surface. This is based on the finding that maximal polarization of cell somata in pyramidal cells is obtained in this orientation [43]. When the target is in a sulcus the preferred direction may be tangential to the skull and perpendicular to the sulcus (e.g. motor cortex). If the target is on a gyrus, then a radial field may be desirable.

7.4. Safety criteria

We have demonstrated that the specifics of the safety criteria (total current, versus limits on individual electrodes) drastically affect the resulting optimal configurations. We have focused on the more conservative safety criterion of limiting the total current. This had the additional advantage of leading to solutions with a small number of electrodes. To reduce hardware complexity it may be useful to modify the proposed approach and explicitly search for the best subset of electrode locations among a large number of candidate locations (say 5 out of 256, if 4 is the available number of independently controlled currents in the stimulator hardware). In doing so, one is implicitly optimizing for location by significantly increasing the density of the electrode arrangement – not with the intention of actually implementing this many electrodes in hardware, but only for the sake of finding optimal locations. In contrast, when limiting currents at individual electrodes one may consider instead montages that ensure a minimum distance between electrodes.

7.5. Indirect optimization of location

Note that we have only indirectly optimized for electrode location. By sampling the space we have maintained linearity and added instead a sparsity constraint. An alternative is to use non-linear optimization and move the electrodes in a continuum of locations [30]. The advantage of the present approach is that the FEM is computationally expensive, while the linear optimization is not. Thus we were able to solve the computationally demanding problem once for a given head (with many electrodes) and then employ efficient linear techniques to optimize for different target locations and orientations in real-time.

7.6. Safety of tissue beyond the brain

The optimization focused only on locations within the brain. This reduced computational complexity and provided clarity to the presentation of the results. Non-brain areas are presumably irrelevant in terms of neuro-modulatory efficacy, but may be relevant in terms of minimizing sensation and skin irritations. However, we know that the largest current intensities occur immediately under the electrode. Previous experimental work with the small gel electrodes modeled here established comfort and skin safety up to 2mA though each electrode [45], which is the worst-case condition.

7.7. Generalization to non-DC current

As mentioned in the introduction, the optimization of applied currents may be performed for any noninvasive electrical stimulation modality. When considering tACS, for example, the permittivity of tissue may not necessarily be neglected as was the case in this paper. Nevertheless, Laplace's equation may be solved for a complex impedance $\sigma + j\omega\epsilon$, where ω is the stimulation frequency and ϵ is the permittivity of the volume. Moreover, when stimulating across multiple frequencies, the electric field solutions at each frequency may be combined linearly across the stimulation bandwidth to yield the net solution. The precise values of tissue impedance (conductivity and permittivity) are the subject of ongoing research [46], [47], [48]. However, it is important to point out that the solution to Laplace's equation (at least in the case of concentric shells) is a function of the ratio of tissue impedances. As such, the absolute values are likely not as consequential as the proportions.

7.8. Potential improvements of optimization algorithms

A vast number of existing algorithms known in the beamforming literature have not been considered in this paper. For instance, LCMV has simplicity as its advantage, but determining the maximum desired field intensity achievable within the maximum current limits is currently an iterative process that could be improved. Moreover, the problem of strong side-lobes is well recognized and a number of algorithms have been proposed to address this issue. Alternative optimization criteria could be conceived. For instance, one may desire maximum intensity in a distributed area or simultaneously at multiple foci. This can easily be incorporated into the WLS approach presented here. Note that somatic polarization scales roughly with the cosine of the applied field direction and the primary cell orientation [43]. Thus, the linear constraint in the LCMV algorithm could be relaxed and made to correspond more directly to cell polarization by specifying only the cosine of the field with the desired direction (by replacing the constraint in (12) with: $\mathbf{e}_o^T \mathbf{C} \mathbf{s} = \alpha \mathbf{e}_o^T \mathbf{e}_o$, where α is a positive scalar). Finally, in brain nuclei that have no preferred orientation, one may be interested in achieving maximum intensity regardless of field orientation, that is, one would constrain or optimize power (no longer a linear constraint). We hope that with the growth of noninvasive electrical stimulation, the

framework established here will lead to the development of more advanced optimization techniques aimed specifically for multi-electrode electrical stimulation.

7.9. Guidelines for the use of conventional electrode configurations

The customarily employed distant bi-polar configuration may be optimal in terms of intensity (at least in the case of a radial target), but certainly not focality. Despite its simplicity, the ad-hoc bipolar configuration considered in this paper is not currently used in practice. We have found that this ad-hoc bipolar configuration is a reasonable approximation to the optimal configuration in the case of a desired tangential field. While in hindsight this solution seems obvious, the dependence of electrode configuration on desired field orientation has so far not been recognized. For example, the 4-by-1 montage is a suitable design for radially oriented currents, but is unlikely to be appropriate for tangential fields. Moreover, in both radial and tangential cases, anatomical idiosyncrasies lead to significant deviations of the optimally focal solution from nominal designs.

Another finding which is intuitively satisfying relates to the location of the maximally intense bipolar configuration. In the case of tangential stimulation, naive placement of large electrodes over the target region misses the point of maximal stimulation, which lies between electrodes and not directly under the pad as commonly assumed. On the other hand, when desiring radial stimulation, one electrode is indeed best placed above the target, with the return electrode positioned at a disparate altitude to properly orient the current flow.

8. Conclusion

This paper has presented a novel, multi-electrode paradigm for non-invasive electrical stimulation in which a patient-specific MRI-based model of the head is utilized to determine the electrode positions and current intensities which optimize the induced electric field in either focality or intensity. It was shown that the optimal stimulation parameters are strongly affected by both the desired field orientation at the target and the optimization criterion (focality or intensity). Moreover, achievable focality is limited by the safety constraint on maximum currents; in the absence of these safety constraints, the maximally focal solution takes the form of a weighted spherical sinc function. On the other hand, it was shown that to maximize target field intensity under an ℓ_1 safety constraint, the optimal configuration is bipolar with ample separation between anode and cathode. The results indicate that both focality as well as intensity at the target can be drastically improved over the conventional approach of using large pad-electrodes. Furthermore, it was shown that ad-hoc approaches employing multiple small electrodes can be also optimized. This is due to the idiosyncratic differences in anatomy which lead to subject-specific “hot-spots” that are difficult to localize without accurate anatomical models. The proposed optimization approach makes systematic use of these individual

differences.

Acknowledgments

This work was supported by The Defense Advanced Research Projects Agency (government contract no. NBCHC080029). We would also like to acknowledge support for this project from the National Science and Engineering Research Council of Canada (NSERC).

The views, opinions, and/or findings contained in this article are those of the authors and should not be interpreted as representing the official views or policies, either expressed or implied, of the Defense Advanced Research Projects Agency or the Department of Defense.

References

- [1] M. A. Nitsche and W. Paulus, "Excitability changes induced in the human motor cortex by weak transcranial direct current stimulation," *Journal of Physiology*, 527.3, pp. 633–639, 2000.
- [2] P. S. Boggio et al., "Go-no-go task performance improvement after anodal transcranial DC stimulation of the left dorsolateral prefrontal cortex in major depression." *J. Affect. Disord.* vol. 101, pp. 9198, 2007.
- [3] P. S. Boggio, P. Liquori, N. Sultani, L. Rezende, S. Fecteau, F. Fregni, "Cumulative priming effects of cortical stimulation on smoking cue-induced craving." *Neurosci. Lett.*, vol. 463, pp. 82-86, 2009.
- [4] F. Fregni, et al., "A sham-controlled, phase II trial of transcranial direct current stimulation for the treatment of central pain in traumatic spinal cord injury." *Pain*, vol. 122, pp. 197209, 2006.
- [5] F. Fregni, S. D. Freedman, A. Pascual-Leone, "Recent advances in the treatment of chronic pain with non-invasive brain stimulation techniques." *Lancet Neurol.*, vol. 6, pp. 188191, 2007.
- [6] F. Fregni, S. Thome-Souza, M. A. Nitsche, S. D. Freedman, K. D. Valente, A Pascual-Leone, "A controlled clinical trial of cathodal DC polarization in patients with refractory epilepsy." *Epilepsia*, vol. 47, pp. 335342, 2006.
- [7] F. Fregni, D. K. Simon, A. Wu, A. Pascual-Leone, "Non-invasive brain stimulation for Parkinson's disease: a systematic review and meta-analysis of the literature." *J. Neurol. Neurosurg. Psychiatry*, vol. 76, pp. 16141623, 2005.
- [8] F. Hummel et al., "Effects of non-invasive cortical stimulation on skilled motor function in chronic stroke." *Brain*, vol. 128, pp. 490-499, 2005.
- [9] J. M. Baker, C. Rorden, J. Fridriksson, "Using transcranial direct-current stimulation to treat stroke patients with aphasia." *Stroke*. vol. 41, no. 6, pp. 1229-36. 2010.
- [10] F. Fregni, P. S. Boggio, M. A. Nitsche, F. Berman, A. Antal, E. Feredoes, et al., 2005a. Anodal transcranial direct current stimulation of prefrontal cortex enhances working memory. *Exp. Brain Res.* 166, 2330.
- [11] M. B. Iyer, U. Mattu, J. Grafman, M. Lomarev, S. Sato, E. M. Wassermann, "Safety and cognitive effect of frontal DC brain polarization in healthy individuals." *Neurology*, vol. 64, pp. 872-875, 2005.
- [12] D. Reato, A. Rahman, M. Bikson, and L. C. Parra, "Low-intensity electrical stimulation affects network dynamics by modulating population rate and spike timing," *Journal of Neuroscience*, vol. 33(45), pp. 15067-15079, 2010.
- [13] A. Datta, V. Bansal, J. Diaz, J. Patel, D. Reato, M. Bikson, "Gyri-precise head model of transcranial DC stimulation: Improved spatial focality using a ring electrode versus conventional rectangular pad." *Brain Stimulation*. vol. 2(4), pp. 201-207, 2009.

- [14] A. Datta, J. M. Baker, M. Bikson, J. Fridriksson, "Individualized model predicts brain current flow during transcranial direct-current stimulation treatment in responsive stroke patient," *Brain Stimulation*, in press, 2011.
- [15] S. Baillet, J. C. Mosher, and R. M. Leahy, "Electromagnetic Brain Mapping." *IEEE Signal Processing Magazine*, vol. 2(6), pp. 14-30, 2001.
- [16] J. Ruohonen, and R. J. Ilmoniemi, "Focusing and targeting of magnetic brain stimulation using multiple coils." *Med Biol Eng Comput.*, vol. 36(3), pp. 297-301, 1998.
- [17] B. D. Van Veen and K. M. Buckley, "Beamforming: a versatile approach to spatial filtering." *IEEE ASSP Magazine*, vol. 5, pp. 4-24, 1998.
- [18] H. Krim and M. Viberg, "Two decades of array signal processing research: the parametric approach." *IEEE Signal Processing Magazine*, vol. 13(4), pp. 67-94, 1996.
- [19] A. Antal, K. Boros, C. Poreisz, L. Chaieb, D. Terney, and W Paulus, "Comparatively weak after-effects of transcranial alternating current stimulation (tACS) on cortical excitability in humans." *Brain Stimulation*, vol. 1, pp. 97105, 2008.
- [20] V. Suihko and H. Eskola, "Transcranial electrical stimulator producing high amplitude pulses and pulse trains." *J. Med. Eng. Technol.*, vol. 22, pp. 211-215, 1998.
- [21] V. Moliadze, A. Antal, W. Paulus, "Electrode-distance dependent after-effects of transcranial direct and random noise stimulation with extracephalic reference electrodes." *Clin. Neurophysiol.*, vol. 121, pp. 2165-2171, 2010.
- [22] A. R. Brunoni, J. Amadera, B. Berbel, M. S. Volz, B. G. Rizzerio, and F. Fregni, "A systematic review on reporting and assessment of adverse effects associated with transcranial direct current stimulation." *Int J Neuropsychopharmacol.*, vol. 15, pp. 1-13, 2011.
- [23] Y. Vandermeeren, J. Jamart, and M. Osseman, "Effect of tDCS with an extracephalic reference electrode on cardio-respiratory and autonomic functions." *BMC Neurosci.*, vol. 16, pp. 11-38, 2010.
- [24] C. Poreisz, K. Boros, A. Antal, W. Paulus, "Safety aspects of transcranial direct current stimulation concerning healthy subjects and patients." *Brain Res Bull.*, vol. 72, pp. 208-214, 2007.
- [25] R. M. Dubinsky RM and J. Miyasaki, "Assessment: efficacy of transcutaneous electric nerve stimulation in the treatment of pain in neurologic disorders (an evidence-based review): report of the Therapeutics and Technology Assessment Subcommittee of the American Academy of Neurology." *Neurology*, vol. 74, pp. 173-176, 2010.
- [26] A. Scott, *The ECT Handbook*. Royal College of Psychiatrists: London, 2005.
- [27] P. C. Miranda, M. Lomarev, and M. Hallett, "Modeling the current distribution during transcranial direct current stimulation," *Clinical Neurophysiology*, 117, pp. 1623-1629, 2006.
- [28] R. N. Holdefer, R. Sadleir, and M. J. Russell, "Predicted current densities in the brain during transcranial electrical stimulation," *Clinical Neurophysiology*, 117, pp. 1388-1397, 2006.
- [29] T. Wagner, F. Fregni, S. Fecteau, A. Grodzinsky, M. Zahn, and A. Pascual-Leone, "Transcranial direct current stimulation: a computer-based human model study," *NeuroImage*, vol. 35, pp. 1113-1124, 2007.
- [30] C. W. Im, H. H. Jung, J. D. Choi, S. Y. Lee, and K. Y. Jung, "Determination of optimal electrode positions for transcranial direct current stimulation," *Physics in Medicine and Biology*, 53, pp. N219-N225, 2008.
- [31] H. S. Suh, W. H. Lee, Y. S. Cho, J. H. Kim, and T. S. Kim, "Reduced spatial focality of electrical field in tDCS with ring electrodes due to tissue anisotropy." in *Proc. IEEE Eng. Med. Biol. Soc.*, vol. 1, pp. 2053-2056, 2010.
- [32] J. H. Park, D. W. Kim, and C. H Im, "A novel array-type transcranial direct current stimulation (tDCS) system for accurate focusing on targeted brain regions." in *Proc. Biennial IEEE Conference on Electromagnetic Field Computation*, 2010.
- [33] D. Griffiths, *Introduction to Electrodynamics*, Prentice-Hall: Upper Saddle River, NJ, 1999.
- [34] D. Logan, *A First Course in the Finite Element Method*. Nelson: Toronto, 2007.
- [35] J. Reilly, *Applied Bioelectricity*. Springer, 1992.

- [36] R. Tibshirani, “Regression shrinkage and selection via the lasso.” *Journal of the Royal Statistical Society*. Vol. 58, pp. 267-288.
- [37] O. L. Frost III, “An algorithm for linearly constrained adaptive array processing,” *Proc. IEEE*, vol. 60(8), 1972.
- [38] D. Alevras and M. W. Padberg, *Linear Optimization and Extensions: Problems and Extensions*, Universitext, Springer-Verlag, 2001.
- [39] P. C. Miranda, P. Faria, and M. Hallett. “What does the ratio of injected current to electrode area tell us about current density in the brain during tDCS?” *Clin. Neurophysiol.*, vol. 120, pp. 1183–1187, 2009.
- [40] M. Grant, S. Boyd, and Y. Ye, “Disciplined Convex Programming.” Chapter in *Global Optimization: From Theory to Implementation*, L. Liberti and N. Maculan (eds.), Springer, pages 155-210, 2006.
- [41] G. H. Golub and C. F. Van Loan, *Matrix Computations*. Baltimore, MD: Johns Hopkins University Press, 1996.
- [42] A. Delorme and S. Makeig, “EEGLAB: an open source toolbox for analysis of single-trial EEG dynamics.” *Journal of Neuroscience Methods*, vol. 134, pp. 9-21, 2004.
- [43] T. Radman, R. L. Ramos, J. C. Brumberg, M. Bikson, “Role of cortical cell type and morphology in sub- and suprathreshold uniform electric field stimulation.” *Brain Stimul.*, vol. 2, pp. 215–228, 2009.
- [44] B. Widrow, K. Duvall, R. P. Gooch, W. C. Newman, “Signal cancellation phenomena in adaptive antennas: causes and cures.” *IEEE Trans. on Antennas and Propagation*, vol. AP-30, pp. 469–478, 1982.
- [45] P. Minhas, J. Patel, V. Bansal, J. Ho, A. Datta, M. Bikson, “Electrodes for high-definition transcutaneous DC stimulation for applications in drug-delivery and electrotherapy, including tDCS.” *Journal of Neuroscience Methods*, vol. 190(2), pp. 188–97, 2010.
- [46] S. Gabriel, R. W. Lau, and C. Gabriel, “The dielectric properties of biological tissue: II. Measurements in the frequency range 10Hz to 20GHz.” *Phys. Med. Biol.*, vol. 41, pp. 2251–2269, 1996.
- [47] N. K. Logothetis, C. Kayser, and A. Oeltermann, “In Vivo Measurement of Cortical Impedance Spectrum in Monkeys: Implications for Signal Propagation.” *Neuron*, vol. 55, pp. 809–823, 2007.
- [48] C. Bédard, S. Rodrigues, N. Roy, D. Contreras, A. Destexhe, “Evidence for frequency-dependent extracellular impedance from the transfer function between extracellular and intracellular potentials.” *J. Comput Neurosci*, vol. 29, pp. 389–403, 2010.

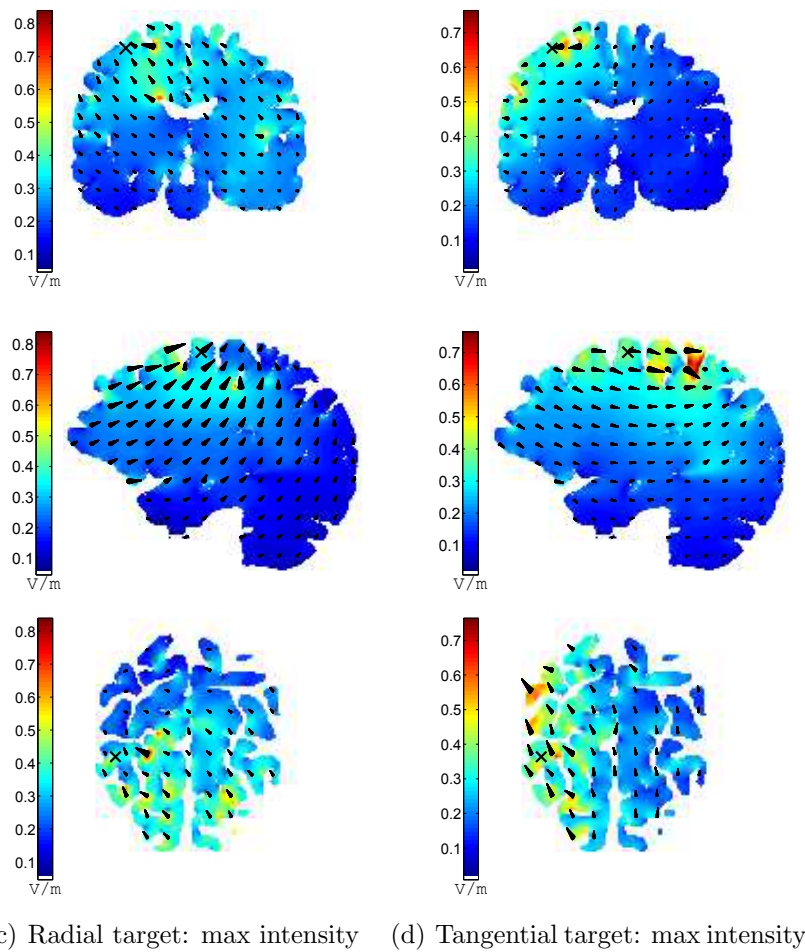
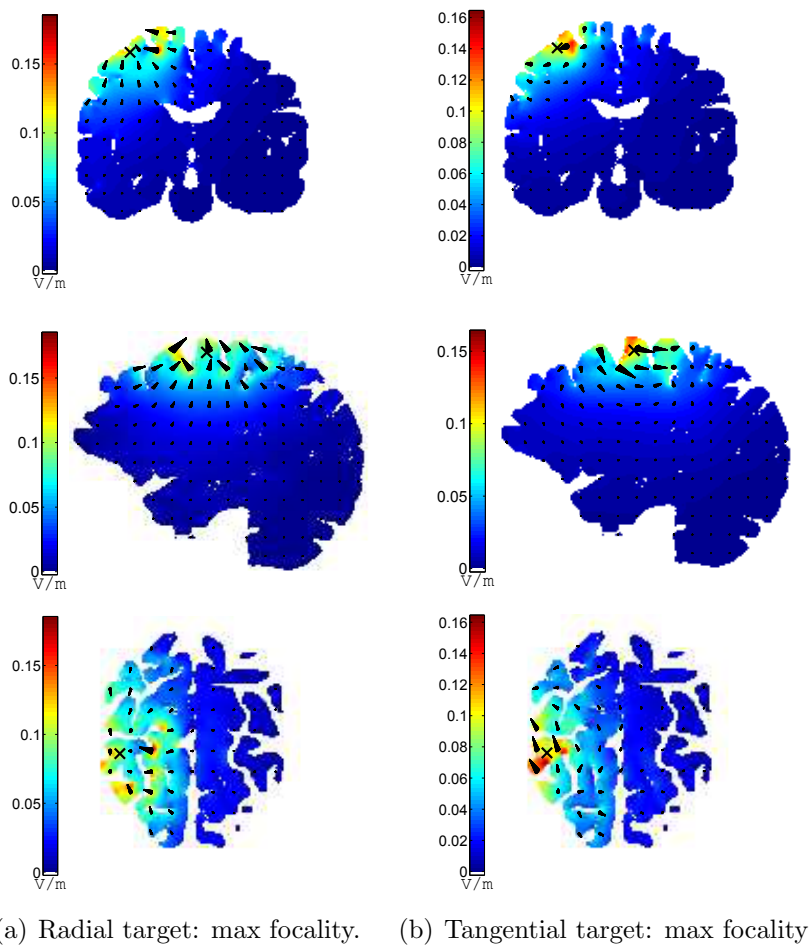
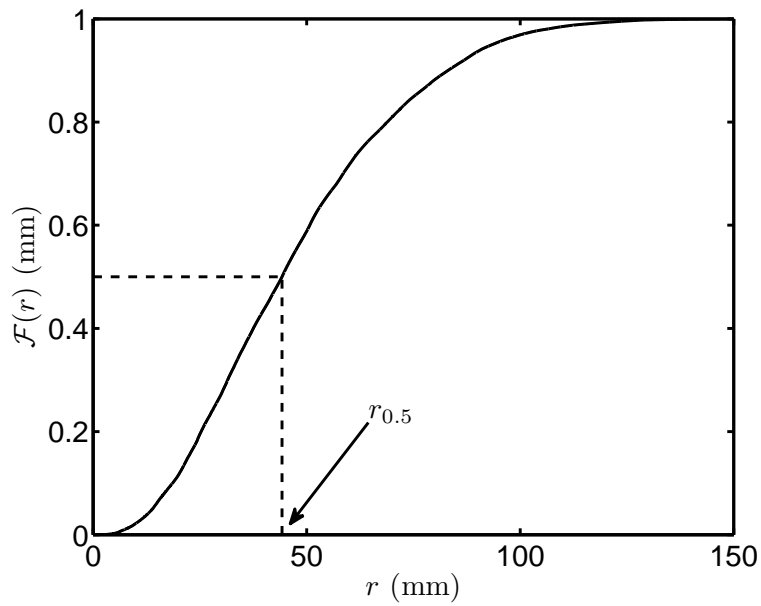
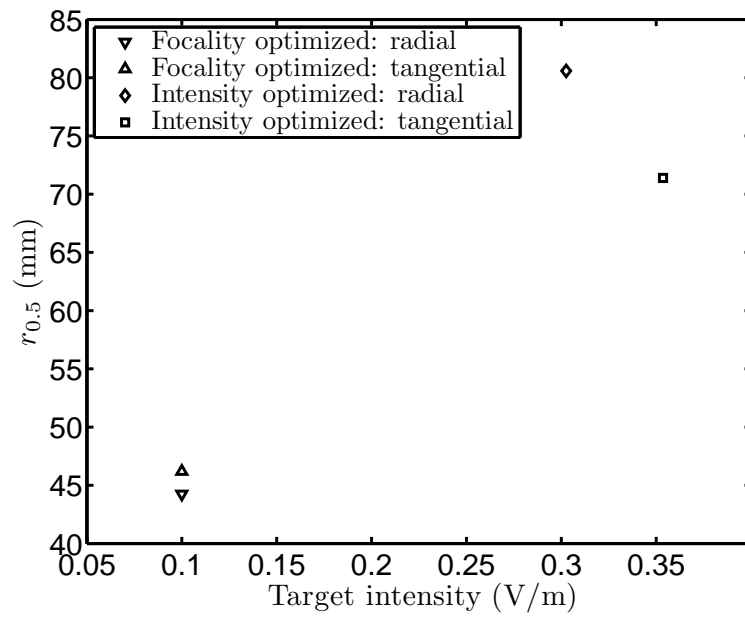


Figure 5. Optimized electric fields for varying orientation and criterion.

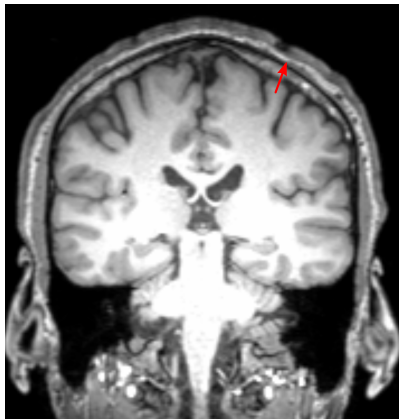


(a) Half-max radius (max focality, radial).

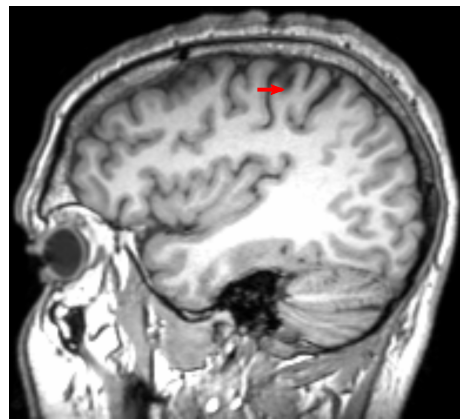


(b) Performance in the focality-intensity space.

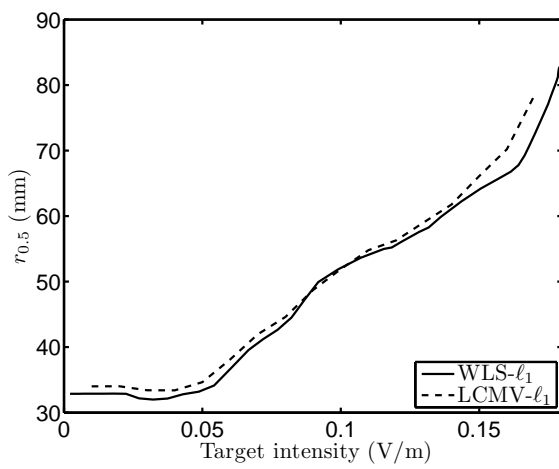
Figure 6. Summary of stimulation results: (a) proportion of electric field contained within a sphere of increasing radius, with $r_{0.5} = 44$ mm; (b) maximizing intensity leads to reduced focality and vice versa .



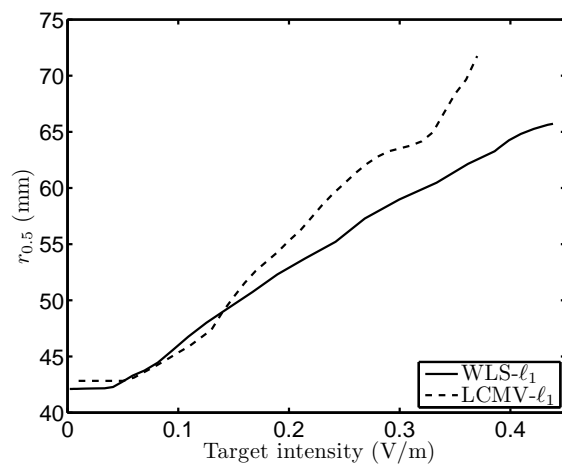
(a) Target employed for radial stimulation.



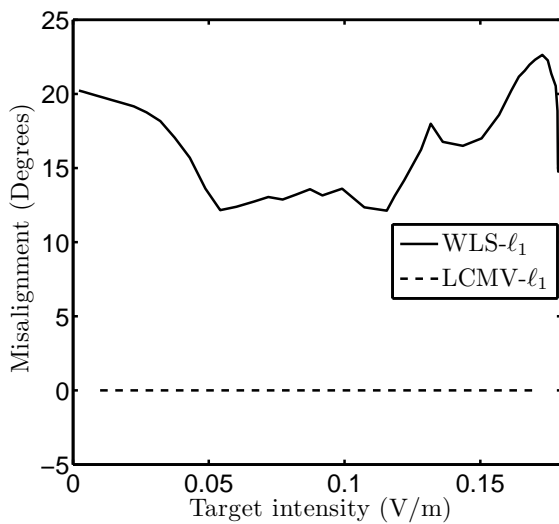
(b) Target employed for tangential stimulation.



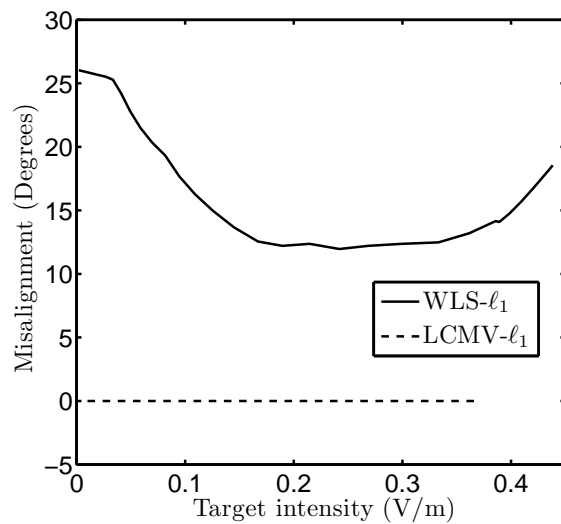
(c) Radial stimulation: focality vs. intensity



(d) Tangential stimulation: focality vs. intensity



(e) Radial stimulation: misalignment



(f) Tangential stimulation: misalignment

Figure 7. WLS is able to achieve larger target intensities above 0.15 V/m while leading to misalignment in the achieved field direction at the target. Otherwise both algorithms give comparable results with tangential fields generally being stronger than radial fields and stronger fields generally being less focal.

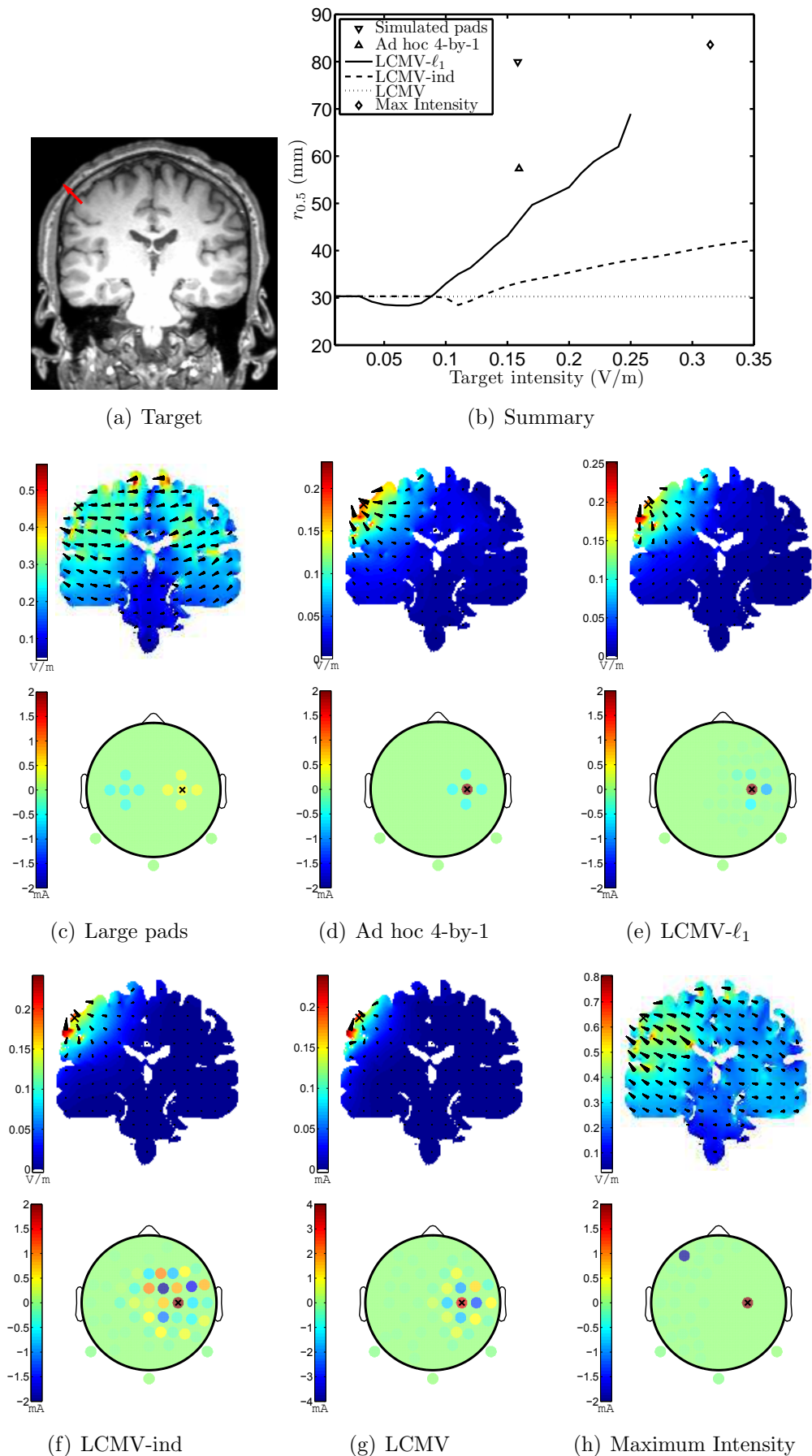


Figure 8. Focality-intensity trade-off and the algorithms that balance them: radial desired field. Electric field slices and optimal current distributions are shown for a target intensity of 0.16 V/m, except in the case of the maximum intensity method, in which the slice corresponds to the maximum attainable intensity of 0.32 V/m.

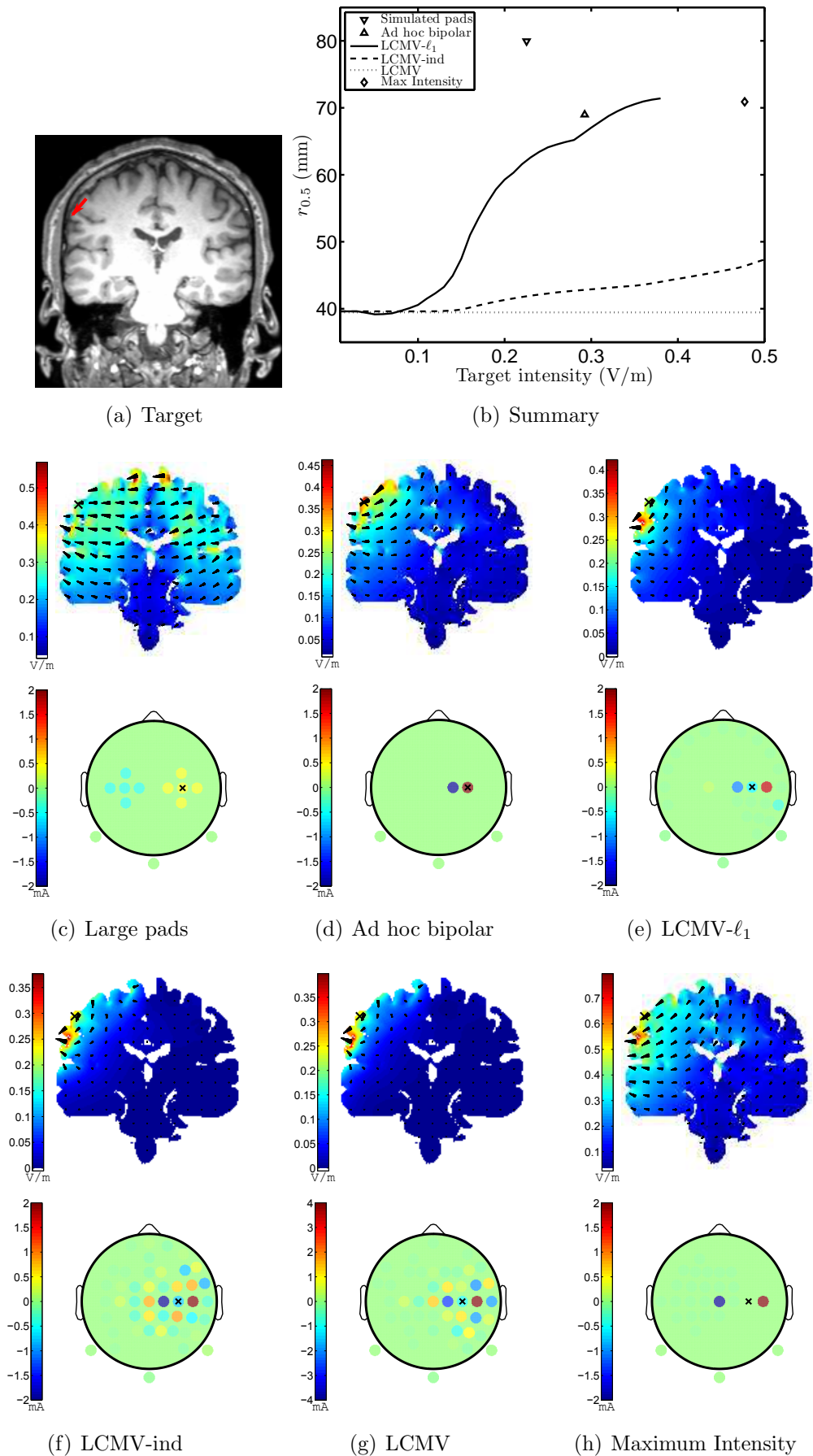


Figure 9. Focality-intensity trade-off and the algorithms that balance them: tangential desired field. In (e) and (f), electric field slices and optimal current distributions are shown for a target intensity of 0.23 V/m.